PERGAMON

Journal of Structural Geology 21 (1999) 837–853

JOURNAL OF STRUCTURAL GEOLOGY

Quantitative kinematic flow analysis from the Main Central Thrust Zone (NW-Himalaya, India): implications for a decelerating strain path and the extrusion of orogenic wedges

Bernhard Grasemann[a,*], Harry Fritz[b], Jean-Claude Vannay[c]

[a]*Institut für Geologie, University of Vienna, Althanstrasse 14, A-1090 Vienna, Austria*
[b]*Institut für Geologie und Paläontologie, University of Graz, Heinrichstraße 26, A-8010 Graz, Austria*
[c]*Institut de Minéralogie et Pétrographie, University of Lausanne, CH-1015 Lausanne, Switzerland*

Received 7 September 1998; accepted 17 March 1999

Abstract

Quantitative kinematic indicators from the Main Central Thrust Zone (MCTZ) in the NW-Himalaya have been used to characterize the type of flow during deformation. Different generations of tension gashes have been rotated by variable angles with respect to the mylonitic foliation, forming associated *fringe folds*. These record the late stage brittle–ductile flow and reveal that a strong pure shear component of deformation occurred throughout the MCTZ. To characterize earlier deformation increments, fabrics from highly deformed quartz ribbons were analyzed. Well-developed shape- and lattice-preferred orientation patterns show a systematic change of the glide systems and suggest inverted palaeotemperatures within the MCTZ. Investigations of the *c*-axes patterns reveal a strong asymmetry at the top of the MCTZ, whereas the samples from the base of the MCTZ show almost perfectly symmetrical Type I crossed girdles. Deformation within the MCTZ probably started close to simple shear flow at higher temperatures, which progressively became a more general shear during cooling, and ended in a pure shear dominated flow during the final stages of brittle–ductile deformation (i.e. a *decelerating strain path*). Using the Higher Himalaya Crystalline as an example, a kinematic model for the extrusion of crustal wedges above major thrust zones is suggested.

1. Introduction

The use of quantitative kinematic indicators has shown that the concept of simple shear and pure shear are just end members of deformation and many natural shear zones deformed by general shear (e.g. Gosh and Ramberg, 1976; Passchier, 1987; Simpson and De Paor, 1993; for a review of the applied methods see Passchier and Trouw, 1996). Most of these analyses rely on the assumption that the ratio of the pure shear to the simple shear strain rates remains fixed throughout deformation. However, the idea that flow parameters may vary systematically with time and that the frequently used assumption of a steady-state deformation is not justified has been discussed recently by a few articles (e.g. Jiang and White, 1995; Fossen and Tikoff, 1997). Yet, most of these ideas are based on strictly theoretical considerations although the principal relevance of non-steady-state deformation studies is supported by natural examples of flow paths (e.g. Passchier, 1990; Wallis, 1992; Simpson and De Paor, 1997).

Fossen and Tikoff (1997) showed by means of forward deformation modeling that a *minimum strain path* can be calculated as a deformation, which starts its history close to simple shear but rapidly changes to a more pure shear dominated flow. Although this idea is still controversial (Fossen and Tikoff, 1998; Jiang, 1998), Simpson and De Paor (1997) demonstrated independently by means of the porphyroclast hyperbolic distribution method that the deformation history of a thrust in the Scandinavian Caledonides probably

* Corresponding author.
E-mail address: Bernhard.Grasemann@univie.ac.at (B. Grasemann)

0191-8141/99/$ - see front matter
PII: S0191-8141(99)00077-2

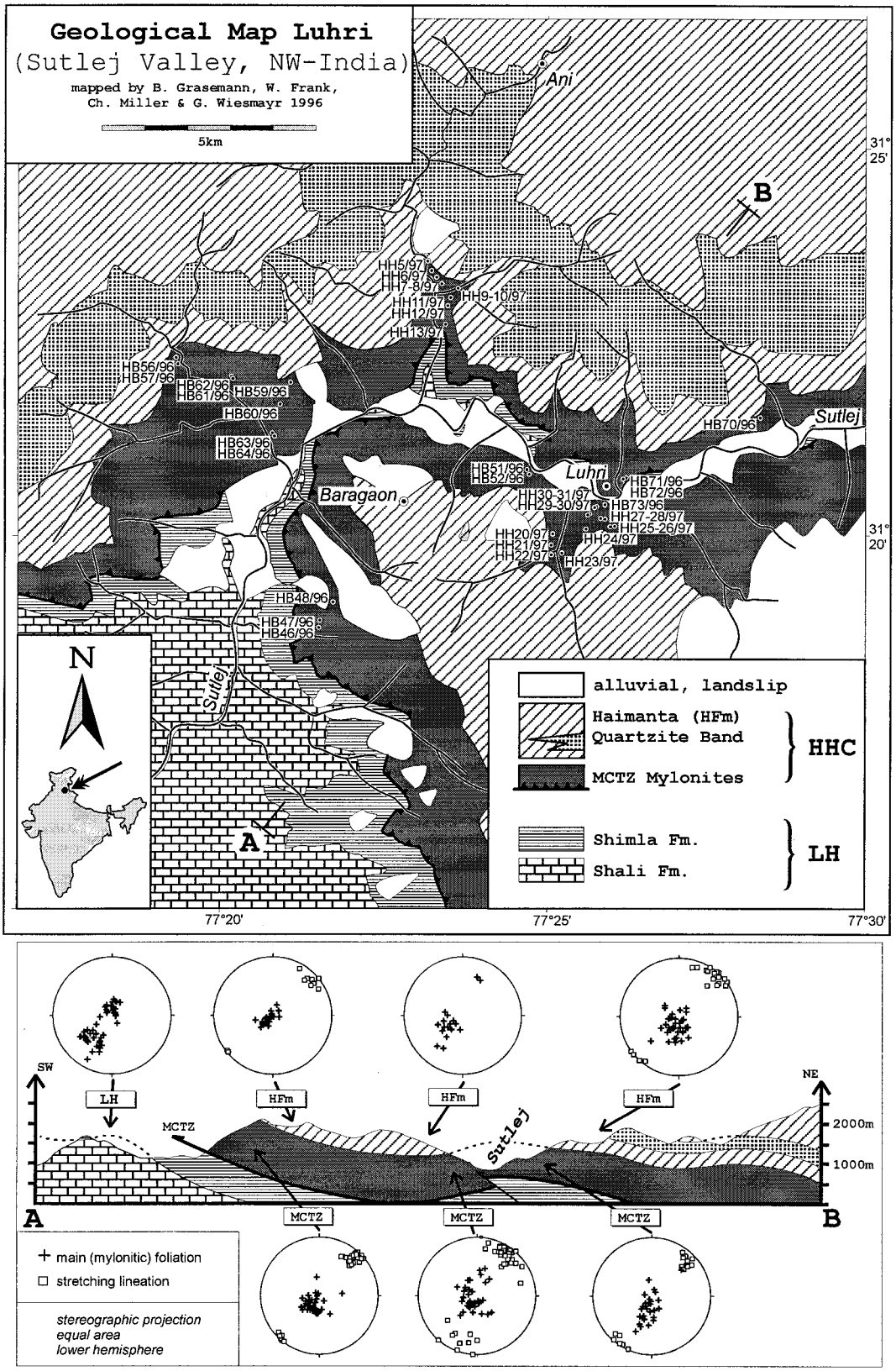

Fig. 1. Geological map of Sutlej Valley around the village of Luhri. The low-grade metamorphosed series of the Lesser Himalaya (LH) are exposed in the Shali half window (West, 1939) in the SW of the mapped area. A brittle detachment at the base of the Main Central Thrust Zone (MCTZ) marks the border to the rocks of the Higher Himalaya Crystalline (HHC), which consist of greenschist to amphibolite facies metamorphic orthogneiss mylonites and of para-series (Haimanta Formation—HFm). Labeled black dots correspond to sampling locations within the MCTZ. A and B mark the orientation of the cross-section. The geological cross-section is roughly parallel to the mylonitic stretching lineation. Stereographic plots show the main planar and linear fabrics associated with the MCTZ deformation.

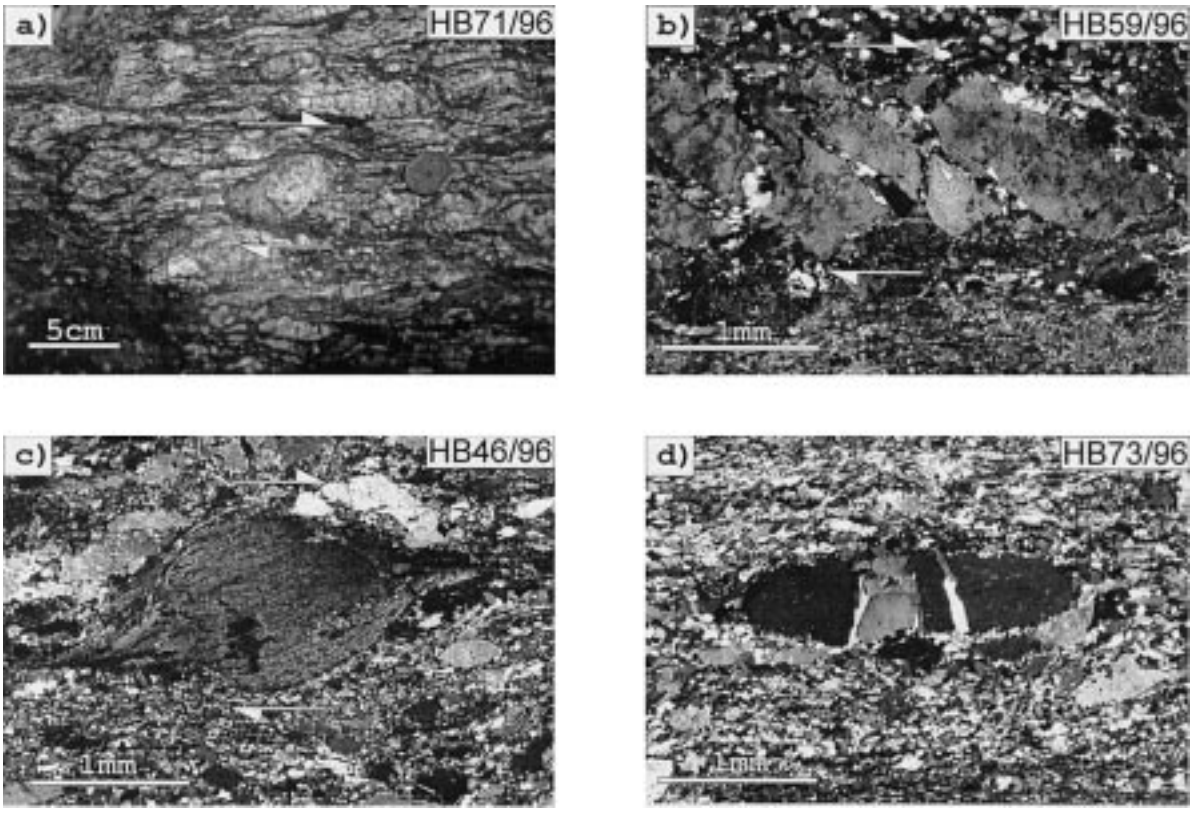

Fig. 2. Orthogneiss mylonites from the MCTZ. Sections are parallel to the stretching lineation, normal to the foliation and have a dextral sense of shear: (a) σ-type porphyroclast of a 5 cm large K-feldspar (HB71/96). (b) Thin section (crossed polarized light) showing synthetic microfaults transecting a K-feldspar. Fragments of the feldspar are boudinaged (HB59/96). (c) Thin section (crossed polarized light) showing mantled σ-type geometry of a 1.5 mm large biotite porphyroclast. Mantles consist of newly formed biotite (HB46/96). (d) Thin section (crossed polarized light) showing micro-boudinage of a K-feldspar. Quartz is recrystallized in large grains in the neck of the boudins (HB73/96).

started close to simple shear and progressively changed to pure shear dominated flow as deformation proceeded.

Based on these ideas, we suggest in this work by means of a new quantitative kinematic indicator and by interpretation of quartz textures, that thrusting along the Main Central Thrust Zone (MCTZ) probably followed such a non-steady-state deformation path. By implementation of such a flow path, a new model for the exhumation of tectonic wedges is discussed.

2. Geology of the MCTZ

In the Sutlej Valley (Fig. 1) mylonitic orthogneisses mark the position of the MCTZ as a major SW-directed thrust zone. Below the basal thrust, low-grade metamorphic Precambrian sedimentary rocks of the Lesser Himalaya (LH) are exposed in the Shali half-window (West, 1939). The brittle detachment at the base of the MCTZ marks the border to the overlying rocks of the Higher Himalaya Crystalline (HHC), which consist of greenschist to amphibolite facies metamorphic orthogneiss mylonites, schists and paragneisses (Haimanta Formation—HFm). Field observations and Rb–Sr whole rock analysis suggest that the protolith of the mylonitic orthogneisses were originally not intrusive into the HFm but rather represent the basement of the metasedimentory rocks (Trivedi et al., 1984; Srivastava and Mitra, 1996). East of the mapped area, the HHC is bordered to the northeast by a normal fault, which correlates with the South Tibetan Detachment Zone (STDZ, Burg et al., 1984). Both the MCTZ and the STDZ were mainly active between 19 and 22 Ma (e.g. Hodges et al., 1992; Dèzes et al., 1999,), although recent studies found younger ages for extensional movements (Hodges et al., 1998 and references cited therein). Because both major fault zones join at a basal detachment (Nelson et al., 1996) it has been suggested that the HHC extrudes with a wedge shape geometry (Burchfiel et al., 1992; Hodges et al., 1993; Grujic et al., 1996).

The flow analysis presented in this work will focus on the ductile to brittle–ductile deformation of the orthogneiss mylonites within the MCTZ. Like in other parts of the Himalayan orogen, the MCTZ is not a discrete plane but a zone of highly deformed rocks up to several km thick associated with an inverted tem-

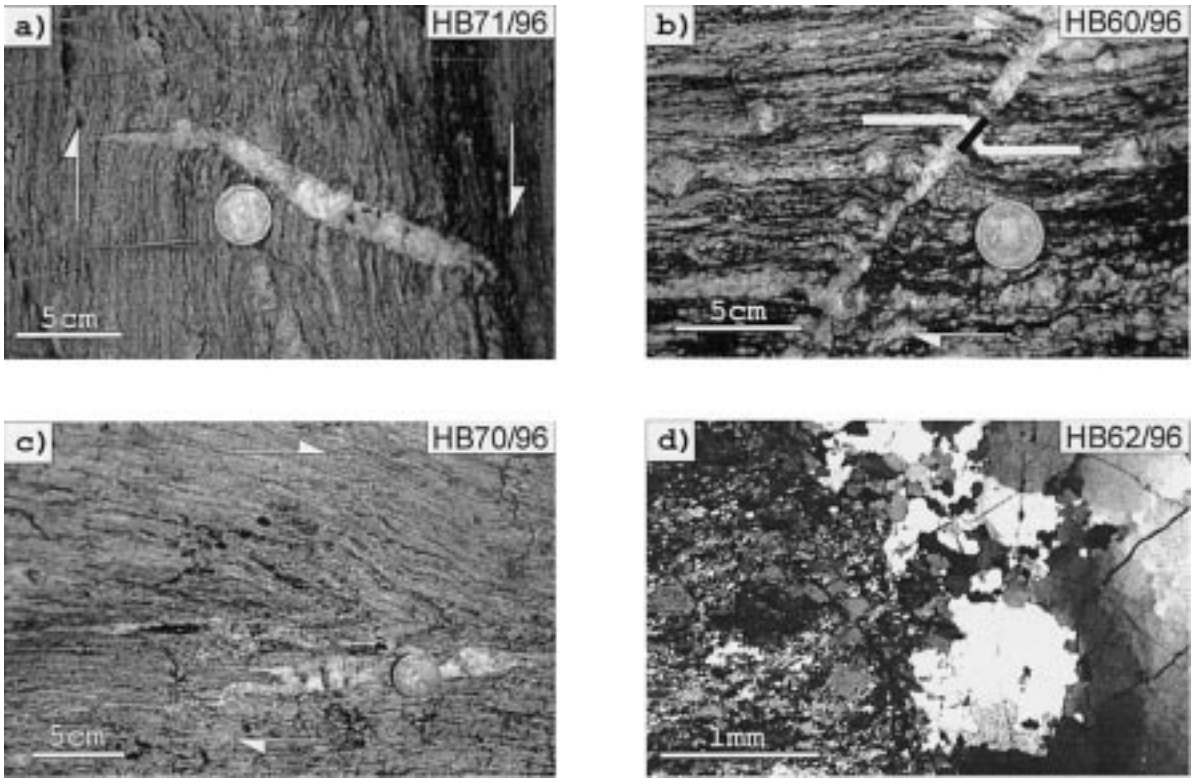

Fig. 3. Extension gashes with associated fringe folds. Sections are parallel to the stretching lineation, normal to the foliation and have a dextral sense of shear: (a) Vein, which has been rotated by an angle of 45°. A younger extension gash propagated at the tip of the older vein has been rotated only by 20° (HB71/97). Note that the veins are slightly folded. (b) Rotated extension gash parallel to the inflexion surface of the synform–antiform pair of fringe folds (HB60/96). (c) Vein, which has been rotated roughly parallel to the mylonitic foliation. Note the nearly isoclinal fold of the associated fringe fold (HB70/96). (d) Thin section (crossed polarized light) showing the contact between the quartz filled vein (right side) and the mylonitic wall rock (left side). Note that the quartz in the vein has suffered dynamic recrystallization indicating ductile deformation of the extension gashes during rotation (HB62/96).

perature gradient (e.g. Hubbard, 1989; Grujic et al., 1996). The main foliation associated with the MCTZ generally dips gently towards the northeast. Although the whole pile was affected by a gentle folding around a NW–SE oriented fold axis, a NE–SW-trending stretching lineation, which reflects the SW-directed shearing along the MCTZ, is well preserved in all units. The up to 1500 m of orthogneiss–mylonites consist mainly of quartz, K-feldspar, plagioclase, biotite and muscovite (Fig. 2) and are typically observed all along the base of the HHC (Frank and Fuchs, 1970; Thöni, 1977; Frank et al., 1995). Shear deformation resulted in a well-defined compositional banding of alternating pure quartz and fine-grained feldspar–phyllosilicate-rich layers. These layers anastomose around less deformed feldspar augen. Feldspar reveals only limited ductile deformation. Recrystallization is mainly by growth of new grains along the edge of feldspar grains or along fractures. Some feldspar porphyroclasts show deformation in the form of patchy undulose extinction or deformation twinning. Larger grains, especially, have been mainly fractured by synthetic and antithetic shear fractures. Retrogressive alteration of feldspar to muscovite and quartz is common and probably associated with the cooling of the MCTZ. Quartz has undergone extensive dynamic recrystallization by subgrain rotation and grain boundary migration developing an oblique foliation. Pure quartz layers show a shape and a lattice preferred orientation.

Abundant shear sense indicators (mantled porphyroclasts, oblique foliation, stair stepping, mica fish, lattice preferred orientation of quartz, antithetic and synthetic microfaults in feldspar grains) with monoclinic symmetry reveal a non-coaxial progressive deformation history of this shear zone with a SW-directed sense of thrusting. At the base of the MCTZ, the transition to the footwall (LH) shows a strong cataclastic overprint. The orientation of striation on slickensides is roughly parallel to the mylonitic stretching lineation, indicating a constant thrusting direction from ductile to brittle deformation.

3. Quantitative kinematic flow analysis of the MCTZ

3.1. Fringe folds

Throughout the MCTZ mylonites quartz-filled ten-

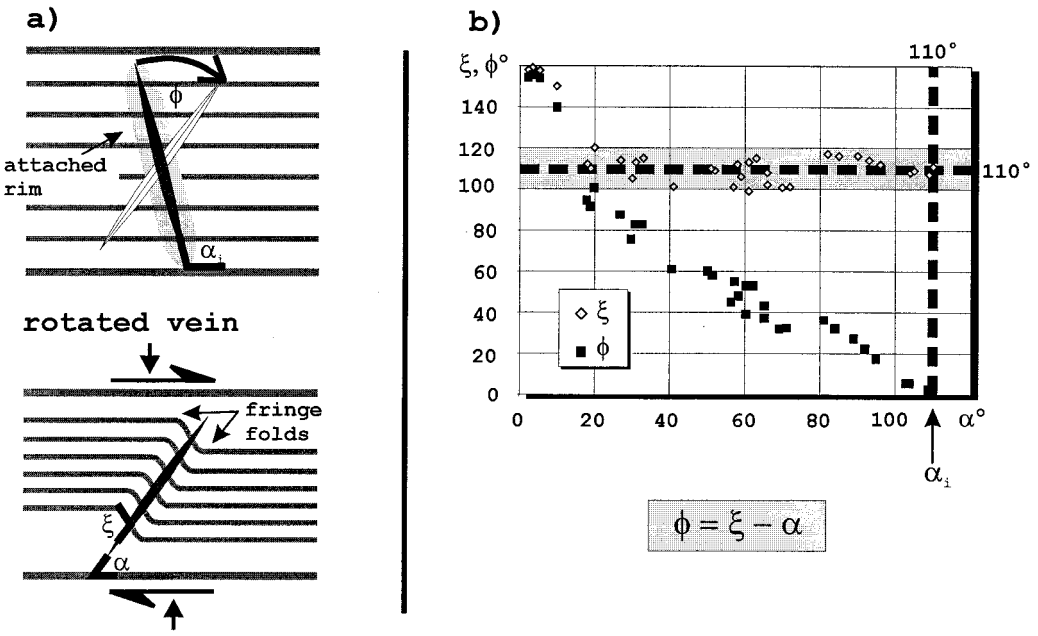

Fig. 4. (a) Model for the formation of extension gashes and the subsequent rotation of the veins by an angle of ϕ. In the vicinity of the veins the original opening angle (α_i) is preserved (ξ). As indicated schematically and developed further in this study the flow is general shear. (b) Plot of the α (angle between the mylonitic foliation and final orientation of the vein) vs ξ (angle between the foliation in the vicinity of the vein and the vein) and ϕ (rotation angle of the vein), respectively. The angle α ranges between a few degrees and 110°, which is supposed to be the original opening angle (α_i). ξ values are fairly constant and scatter around 110°.

sion gashes can be observed (Fig. 3). These gashes always crosscut the foliation and follow the inflexion surface of a fold with a synform–antiform pair resembling structures described by Hudleston (1989) as *paired hook-shaped asymmetric folds* or by Passchier (1997; personal communication) as *fringe folds*. During continuous deformation, the gashes have been rotated by variable angles with respect to the mylonitic foliation. Dynamic recrystallization of quartz within the veins mainly by grain boundary migration suggests that although the gashes opened by brittle fracturing, further deformation occurred within a ductile flow. The angle between the mylonitic lineation and the trace of the tension gashes on the main foliation is roughly perpendicular. Several vein-systems reveal different generations of tension gash formation: older central parts of the veins have rotated in the bulk flow, while younger outer parts still propagate outward (Fig. 3a).

The initial veins probably formed in a similar environment like the *foliation boudinage* described in strongly foliated quartzo-feldspathic schists (Platt and Vissers, 1980). The formation of foliation boudinage is suggested to be controlled by the presence of a pre-existing anisotropy. Two types of foliation boudinage have been described: (i) *Symmetric boudinage* formed by fractures roughly normal to the foliation. Differential extension along the foliation resulted in openings, which were filled with coarse-grained quartz with no sign of internal deformation. (ii) *Asymmetric boudinage* developed where the rock has broken along surfaces oblique to the foliation. No veins developed because displacement was roughly parallel to the synthetic shear fracture. Other similar structures like *ghost foliations* or folding of foliations with axial surfaces parallel to dykes and veins have also been described from different localities (e.g. Rice, 1986; Passchier and Urai, 1988; Druguet et al., 1997). Their formation has been explained by perturbation of flow pattern, competence contrast or polyphase shear deformation.

Hudleston (1989) showed examples of paired hook-shaped folds along veins and fractures in glaciers and high-grade rocks. These folds have a sense of asymmetry on both sides of the veins consistent with the overall sense of shear. However, the sense of offset along the veins is always of the opposite sense to that of the sense of shear predicted by the fold asymmetry. Based on analogue experiments using a Plasticene block, Hudleston (1989) concluded that the formation of the folds was a consequence of the strain in the host material that accommodated the initial fracture and/or the perturbation of flow by the presence of an open, partly healed or filled fracture.

The fringe folds from the MCTZ clearly differ from the above mentioned structures. The veins are tension gashes, which were filled with quartz and show no evidence of a shear component parallel to the vein margins, resembling the symmetric boudinage type.

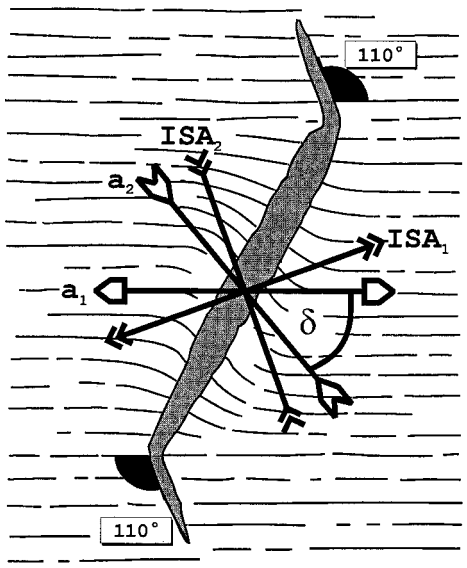

Fig. 5. Geometrical relationship between the fringe folds and the instantaneous stretching axes (ISA_1 and ISA_2) and the flow apophyses (a_1 and a_2). For a detailed explanation see text.

However, the initial opening of the gashes was not normal but oblique to the foliation, probably suggesting that the initial fractures opened normal to the maximum instantaneous extension direction (Ramsay and Huber, 1983).

In order to develop a model for the original orientation of the tension gashes and their subsequent rotation within the MCTZ flow, we measured the orientations of 33 fringe folds (Fig. 4): (i) α is the angle between the mylonitic foliation and the rotated tension gash (anti-clockwise sense). (ii) ξ is the angle between the rotated mylonitic foliation in the vicinity of the gash (i.e. common limb of the antiform–synform pair) and the rotated tension gash (anti-clockwise sense) and (iii) ϕ is the rotation angle of the tension gash or simply $\phi = \xi - \alpha$. Although there is a great variability of α between 0° and 110°, ξ is fairly constant around 110°. Furthermore the largest values for α ($=\alpha_i$), which are found for the youngest gashes in the outer part of older rotated veins, are also around 110° (Figs. 3 and 5). An exception occurs where the veins have rotated nearly into parallelism with the mylonitic foliation ($\alpha<10°$). In that case nearly isoclinal fringe folds developed with ξ angles between 140° and 160°. This observation probably suggests that at low α-values shearing along the margins of the vein takes place, as suggested by Hudleston (1989). The youngest generation of veins shows no evidence of rotation and folding of the foliation. Thus the opening angle of the folds is clearly a function of the rotation component during deformation: gashes that underwent only limited rotation have open folds, whereas larger rotations have resulted in nearly isoclinal folds (Fig. 3). All these observations, especially the fact the throughout the whole mapped area no vein has been found with an $\alpha > 110°$, suggest that the initial opening angle α_i of the veins was around 110°. To conclude, the following mechanism is suggested to explain the observed fringe folds within the MCTZ:

1. The veins formed at a late stage of the flow throughout the MCTZ and crosscut the earlier formed mylonitic foliation. Brittle failure during ductile flow was either due to a limited rate of extension parallel to the mylonitic foliation (Platt and Vissers, 1980), strain hardening at a late stage of mylonitic deformation (Poirier, 1980), periods of rapid strain rates or local stress concentrations caused by heterogeneities and growth of fractures preferentially perpendicular to the least compressive stress (Olson and Pollard, 1991).
2. During shear deformation older veins rotated in bulk flow while new tension gashes developed in the direction of the minimum instantaneous stretching axes (ISA_2, Passchier and Trouw, 1996). However, the veins from the MCTZ do not exhibit the sigmoidal shapes described for the progressive development of tension fissures from brittle ductile-shear zones (Ramsay and Huber, 1983). Probably the opening of the veins within the MCTZ was the result of several rapid successive events rather than continuous fracture propagation during flow.
3. The formation of fringe folds, where no shear across the vein is observed and where the original angle between the mylonitic foliation and the veins has been preserved, irrespective of the amount of finite rotation of the vein, is difficult to explain and requires special conditions (Hudleston, 1989; Passchier, personal communication). Obviously, the folds around the vein must have been developed by a relative rotation of the vein, together with the foliation in the vicinity of the vein. Although no visible zone of alteration along the fringe of the investigated veins has been observed, the formation of similar structures have been explained by hardening of the wall rock in the vicinity of the vein (Passchier, personal communication) or by incorporation of a 'stiff pressure shadow' (Hudleston, 1989) and subsequent relative rotation of the vein and the attached rim.

The fairly constant values of the angle ξ for different generations of veins and the same derived value for α_i imply that the angle between the *ISA* and the mylonitic foliation remained fairly constant during the late stage of deformation. Thus, during the time of the formation of the tension gashes the foliation had already been rotated nearly parallel to the fabric attractor (Fig. 5). Therefore, for the period of vein formation

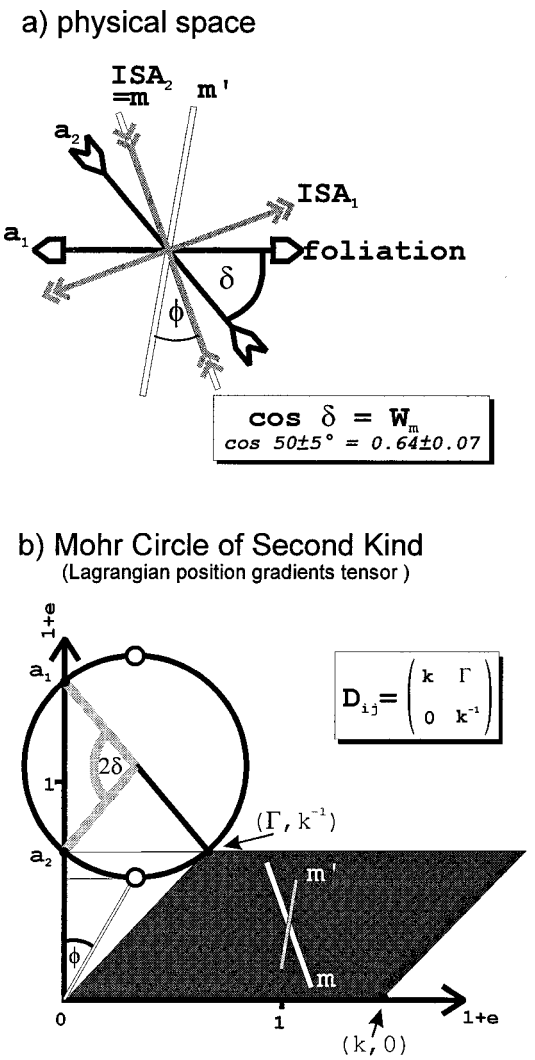

Fig. 6. (a) Physical space and geometric orientation of the instantaneous stretching axis (ISA_1 and ISA_2), the eigenvetors (a_1 and a_2) of flow. The newly formed vein m, which is parallel to the ISA_2 rotated during deformation to an orientation m' by an angle of ϕ. The cosine of the angle between the eigenvectors (δ) gives the mean vorticity number W_m. (b) Mohr circle construction of the position gradient tensor ($\mathbf{D}_{ij}$) for the flow that rotated m to m' with a W_m equal to the cosine of δ. $\mathbf{D}_{ij}$ can be expressed in terms of the pure shear component k and the effective shear strain Γ, which is a function of k and the simple shear component. Large white dots on the Mohr circle indicate the orientations of the ISA_1 and ISA_2 before deformation. The veins m opened parallel to the ISA_2. The rotation of m to m' and the stretch of this line can be read as the polar coordinates of this point.

and subsequent rotation, the late stage flow within the MCTZ is considered to be steady-state, which requires that the flow parameters such as the velocity field, flow apophyses, kinematic vorticity number and instantaneous stretching axes did not change during deformation (Bobyarchick, 1986). For steady-state deformations, the infinitesimal deformation parameters can be deduced from the orientation of the finite deformation parameters. If these assumptions are valid for the observed veins within the MCTZ, and if the flow during formation and rotation of the veins was isochoric plane strain flow, the angle between the original propagation direction of the veins and the mylonitic foliation can be used as a quantitative kinematic indicator for that stage of deformation (Passchier and Trouw, 1996; Passchier, 1997).

Fig. 6(a) shows the orientation of the instantaneous stretching axis (ISA_1 and ISA_2), the eigenvectors (a_1 and a_2) of flow and the vein before (m) and after (m') deformation in the physical space. The marker line m represents the vein, which opened parallel to the ISA_2 and rotated during deformation to an orientation m' by a rotation-angle ϕ. Because the fringe folds formed at a late stage of the MCTZ deformation, the mylonitic foliation is assumed to be nearly parallel to a_1 at the beginning of the formation of the tension gashes. This assumption is justified by the observation that the angle between the initial orientation of the veins and the mylonitic foliation (i.e. α_i) has been constant for different generations of veins. The orientations of the ISA with respect to a_1 can be used to derive the second eigenvector a_2. The cosines of the angle δ between the two eigenvectors give the *mean vorticity number* W_m of the flow (Bobyarchick, 1986; Passchier, 1986), which describes the mean degree of non-coaxiality ($W_m = 0$ for pure shear, $W_m = 1$ for simple shear) for the investigated deformation period. For the assumptions of isochoric plane-strain steady-state flow used in this study, W_m is equal to the kinematic vorticity number W_k (Truesdell, 1954). For the 33 investigated veins within the MCTZ, the angle δ is about $50 \pm 5^\circ$ and consequently W_m between 0.57 and 0.71, indicating a significant component of pure shear deformation.

Finite deformation is conveniently described by a forward Lagrangian position gradient tensor $\mathbf{D}_{ij}$ relating the position of any material point in the deformed state to coordinates in the undeformed state. De Paor and Means (1984) have shown that for any tensor with components D_{11}, D_{12}, D_{21} and D_{22}, points (D_{12},D_{22}) and (D_{21},D_{11}) in Mohr space specify a diameter of a corresponding Mohr circle of the Second Kind such that the Mohr circle is fully determined. A marked property of Mohr circles of the Second Kind is that they can be brought into coincidence with geographic space. Polar coordinates of points on the Mohr circle represent the stretches and rotations of material lines in real space (Means, 1982). In addition, initial angles between two material lines appear as double angles measured along the circle. The intersection of the Mohr circle with the vertical reference axis (0,a_1) and (0,a_2) represents the eigenvector of the flow. The orientation of the eigenvector a_1 is fixed to the flow plane of the simple shear component, but the other eigenvector a_2 has an orientation that is dependent on the rotational and irrotational contributions to general

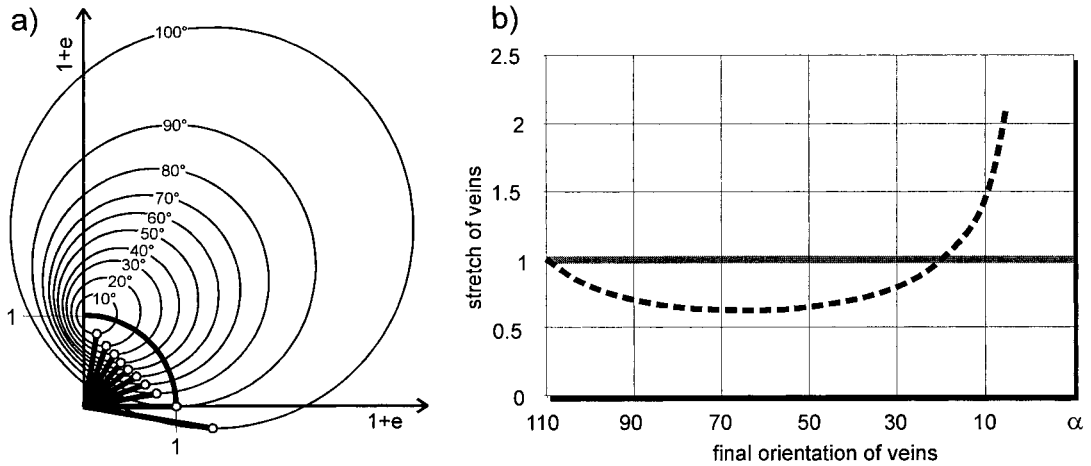

Fig. 7. (a) Mohr circles for finite deformations after the vein formation and subsequent rotation of the veins ($10°<\phi<100°$). Polar coordinates of the white dot and the gray line indicate the rotation angle ϕ and the stretch of the veins. (b) Plot of the final orientations of the rotated veins α vs stretch of the veins. At $\alpha = 110°$ and 20° the veins have a stretch of 1. Between $110°<\alpha<20°$ the veins are shortened. Only for rotations of more than $\phi > 90°$ the veins are elongated.

shear. The larger the pure shear component, the larger the angle 2δ between a_1 and a_2. In physical space the shear zone boundary is parallel to the horizontal reference axis. The deformed normal to the shear zone boundary intersects the Mohr circle at the anchor point (Γ,a_2), being the only point representing a stretched line simultaneously in geographical and strain space (Simpson and De Paor, 1993). With such a reference frame and excluding volume change the position gradient tensor $\mathbf{D}_{ij}$ has the form:

$$D_{ij} = \begin{bmatrix} k & \Gamma \\ 0 & 1/k \end{bmatrix}, \tag{1}$$

where the off-diagonal term is termed *effective shear strain* Γ and can be expressed as a function of both pure and simple shear components (Merle, 1986; Tikoff and Fossen, 1993):

$$\Gamma = \frac{\gamma k^2 - \gamma}{2k \ln k}, \tag{2}$$

where γ is the simple shear and k the pure shear component. In the Mohr circle plot the distance from the origin to the point $(0,a_1)$ is equal to k whereas the distance from the origin to the point $(0,a_2)$ is equal to $1/k$.

As discussed above the fringe folds from the MCTZ indicate a fairly constant W_m. Therefore it is more convenient to express the effective shear strain in terms of the angle δ between the eigenvectors. From the triangle $(0,a_1)$, $(0,a_2)$ and (Γ,a_2) it follows that (Fig. 6b):

$$\Gamma = (k - 1/k)\cot\delta. \tag{3}$$

Furthermore, a trigonometric relationship between $\Gamma/2$ and the rotation of a material line about ϕ exists (Fig. 6):

$$\frac{\Gamma}{2} = \frac{\frac{\left(k + \frac{1}{k}\right)}{2} - \frac{\left(k - \frac{1}{k}\right)}{2\sin\delta}}{\cot\phi}. \tag{4}$$

Solving Eqs. (3) and (4) for k and eliminating Γ:

$$k = \sqrt{\frac{\cos(\phi - \delta) + \sin\phi}{\cos(\phi + \delta) + \sin\phi}}. \tag{5}$$

Thus, all components of the position gradient tensor $\mathbf{D}_{ij}$ can be calculated if δ and ϕ are known. Note that $\mathbf{D}_{ij}$ reconstructed in this way describes only the part of the total deformation during which the veins formed and rotated.

The Mohr circle in stretch space can also be used to construct the deformation parameters geometrically. Starting with a circle of arbitrary diameter, the angle between the eigenvectors plotted as 2δ and the known rotation ϕ of a material line initially parallel to the ISA_2 can be used to find the origin of the Mohr space reference frame. Assuming isochoric flow, the dimensions of the reference frame can be calculated from the deformed unit-square. The lower right and the upper left point of the deformed unit-square represent the tensor components (D_{11},D_{21}) and (D_{12},D_{22}), respectively. In Fig. 6(b) an example of this method is given for a vein which has rotated by $\phi = 30°$ in a flow where $\delta = 50°$.

For the veins within the MCTZ ϕ varies between 0° and 100° (Fig. 4). Furthermore, the constant angle between the veins and the rotated mylonitic foliation

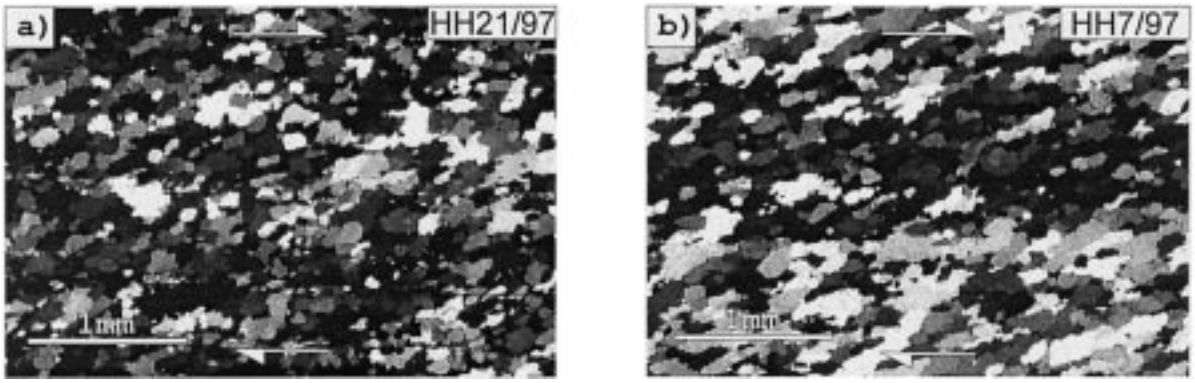

Fig. 8. Thin section (crossed polarized light) of quartz textures. Sections are parallel to the stretching lineation, normal to the foliation. A strong lattice and shape preferred orientation are preserved and reveal a dextral sense of shear (i.e. SW directed thrusting). Sample HH21/97 (a) is from the upper structural level of the MCTZ. Although the elongated quartz grains define a second foliation the ellipticity of the single grains is distinctly less than in sample HH7/97 (b) from lower structural levels.

in the vicinity of the gash (ξ) suggests that the *ISA* had a fixed orientation relative to the mylonitic foliation during the different stages of vein formation. Therefore Mohr circles for the different amounts of rotation of the veins and thus different finite strain can be plotted. Steady-state accumulation of strain is represented by a series of circles with increasing radii. The center of the circle shifts during deformation and follows a path that is dependent on W_m (e.g. Passchier, 1988). Fig. 7(a) shows the Mohr circles for veins opening perpendicular to the ISA_1 and deforming within a flow with $W_m = 0.64$. The polar coordinates of the dots (i.e. orientation of the ISA_2 before deformation) give the rotation ($\phi = 10$–100°) and the stretch of the veins. Due to the opening of the tension gashes parallel to the ISA_2 the veins are shortened during their rotation for $0^\circ < \phi < 45^\circ$, corresponding to an angle between the mylonitic foliation and the gashes of $110^\circ > \alpha > 65^\circ$ (Fig. 7b). Rotating towards the fabric attractor, the veins are elongated until they reach their initial length at $\alpha = 20^\circ$. Only if $\alpha < 20^\circ$ would the veins elongate. These results fit to the field observation that most rotated veins from the MCTZ do not reveal any sign of elongation, except those which have been rotated nearly parallel to the mylonitic foliation (Fig. 3c).

From these investigations of the formation and rotation of fringe folds from the MCTZ, the following conclusions can be drawn: (i) Fringe folds formed at a late stage of ductile deformation throughout the MCTZ with roughly the same kinematics as the overall SW-directed thrusting movement. (ii) Assuming plane strain isochoric flow, the fringe folds can be used as quantitative kinematic indicators suggesting that this late stage of thrusting was controlled by a significant pure shear component.

3.2. Quartz textures

Well-developed *c*-axis fabrics can be used to characterize the kinematics of the associated flow (e.g. Lister and Hobbs, 1980; Schmid and Casey, 1986). In order to get some additional information about the flow parameters controlling the MCTZ thrusting prior to tension gash formation, highly deformed pure quartz ribbons occurring throughout the orthogneiss mylonites were analyzed using an X-ray texture goniometer.

Polished rock chips were placed in the X-ray beam of a texture goniometer (wavelength CuKα = 1.5418, beam current = 40 kV and 30 mA) used in reflection mode. Eight lattice planes ($\langle 100\rangle$, $\langle 110\rangle$, $\langle 102\rangle$, $\langle 200\rangle$, $\langle 201\rangle$, $\langle 112\rangle$, $\langle 211\rangle$, $\langle 113\rangle$) have been directly measured at angles between 0° (center) and 80° (periphery), corrected for defocusing effects and completed (0–90°) by Fourier analyses. Lattice planes $\langle 001\rangle$, $\langle 101\rangle$ and $\langle 011\rangle$ were calculated using the orientation density function (ODF) based on the harmonic method of Roe (1965) and Bunge (1969). Thirty-one samples from different structural levels have been measured throughout the MCTZ. Representative $\langle a\rangle$-axes ($\langle 110\rangle$) and *c*-axes ($\langle 001\rangle$) orientation distributions from different structural levels are shown later as pole figures in Fig. 9. For detailed description of the technical procedure see Wenk (1985).

Quartz has undergone extensive dynamic recrystallization and forms well-developed lattice and grain shape preferred orientation patterns (Figs. 8 and 9). Deformation mechanisms include dynamic recrystallization by grain boundary migration as well as subgrain rotation. The degree of ellipticity of single quartz grains increases from upper to lower structural levels (compare Fig. 8a and b), whereas the angle between the long axis of the ellipse and the foliation decreases

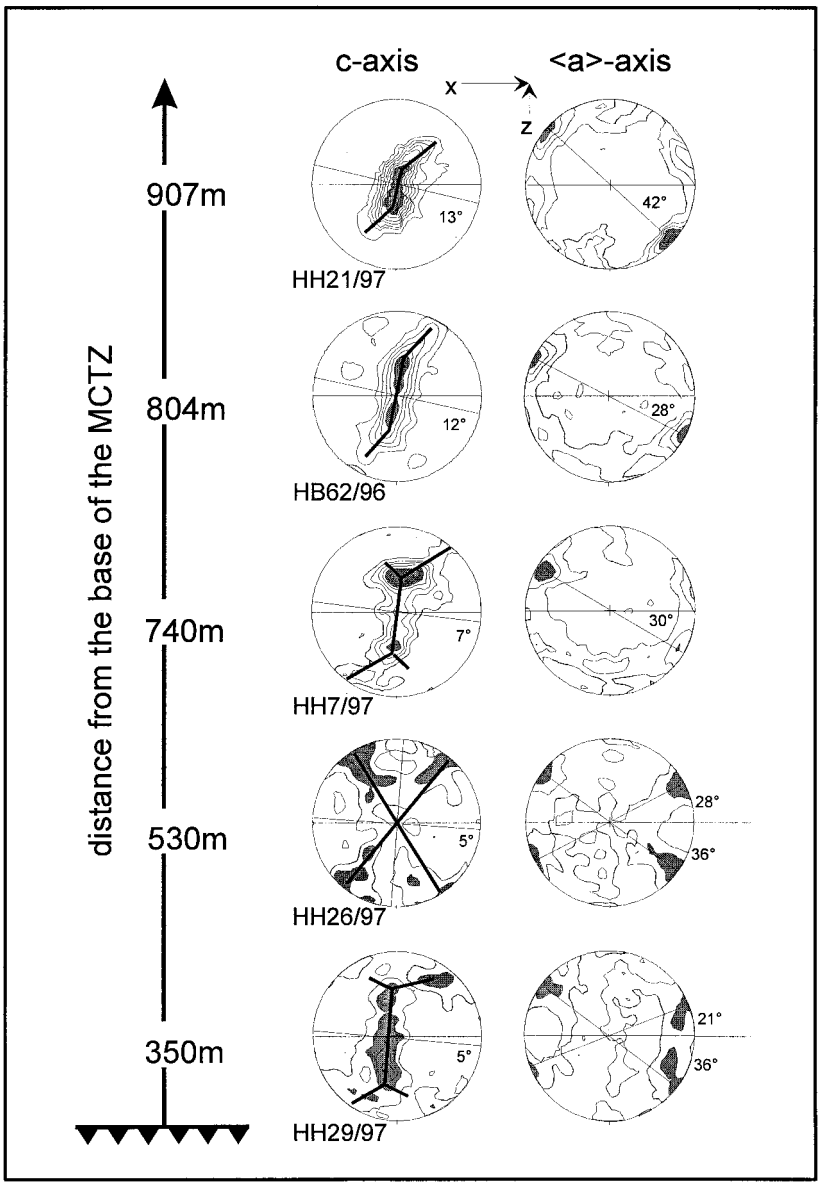

Fig. 9. Stereographic plots of *c*-axes and ⟨*a*⟩-axes distributions (analyses from X-ray textural goniometry, calculation by orientation distribution function, ODF) across the MCTZ. Spacing of contour intervals is one multiple of random (MRD). The angle between the trace of the foliation and the normal to the central girdle of the *c*-axes reveals an increase in the asymmetry of the patterns from the base to the top of the MCTZ. A systematic change of glide systems is interpreted to record an inverted temperature gradient within the MCTZ.

towards the base of the MCTZ probably reflecting different strain geometries (Herwegh and Handy, 1998). Lattice preferred orientation pattern is displayed in pole figures of *c*- and ⟨*a*⟩-axes (Fig. 9). In the fabric diagrams, the maximum extension direction *X* is oriented E–W, *Y* is the center and *Z* is N–S. Most samples except from the base of the MCTZ developed an obliquity of the central girdle segment with respect to the foliation trace (external asymmetry) and an unequal inclination of the peripheral legs with respect to the central girdle segment (internal asymmetry). Some samples show modifications like one or two missing fabric legs. From the systematic variations of *c*-axes and ⟨*a*⟩-axes patterns the following observations have been made:

(1) In all cases ⟨*a*⟩-axes are distributed along the periphery of the stereonet. Accepting models that predict ⟨*a*⟩-axes to represent direction of flow, deformation close to plane strain is suggested (Lister and Williams, 1979).

(2) Lattice preferred orientation patterns suggest systematic change of glide systems from prism ⟨*a*⟩ glide (upper structural levels of the MCTZ) over rhomb ⟨*a*⟩ glide towards contribution of basal ⟨*a*⟩ glide in MCTZ footwall units. Accepting the models, which suggest that with increasing temperatures prism ⟨*a*⟩ slip

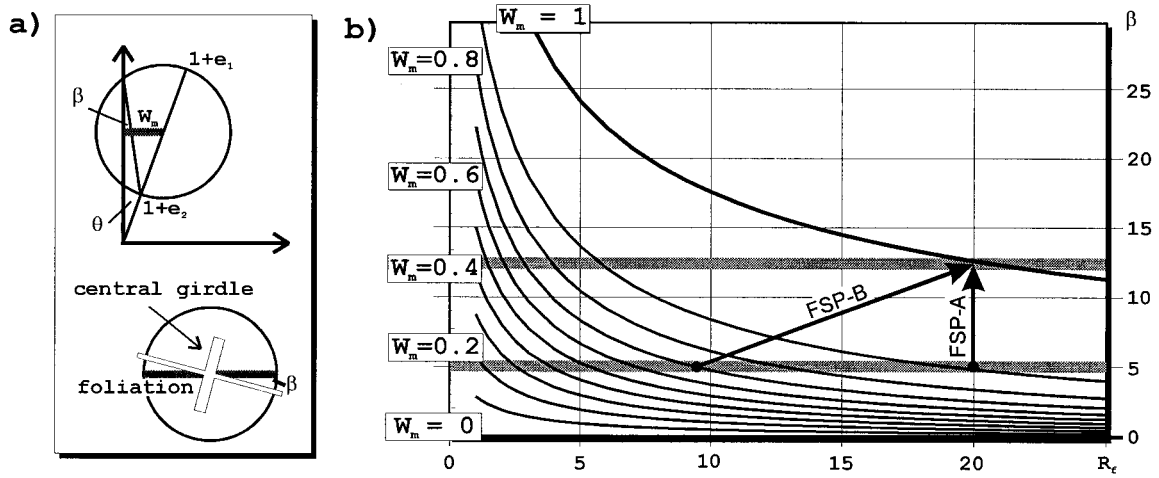

Fig. 10. Vorticity analysis using quartz textures. (a) Trigonometric relationship [Eqs. (6)–(8)] of the angle between the normal to the central girdle and the foliation (β), the finite strain ($1+e_1$,$1+e_2$) and the mean vorticity number (W_m). (b) Plot showing the ellipticity of the finite strain ellipsoid (R_f) vs β for different W_m. Arrows indicate two hypothetical finite strain profiles (FSP) across the MCTZ where the dots represent the R_f values at the base the arrows at the top of the section. In FSP-A the whole profile reveals the same ellipticity of the finite strain ellipsoid. As it is discussed in the text a profile similar to FSP-B is more likely where the lower structural levels record lower R_f values than the top of the MCTZ.

becomes more important and the girdle tends to define a maximum around the *Y*-axis (Wilson, 1975; Bouchez, 1977; Lister and Dornsiepen, 1982; Law, 1990), our results can be interpreted to correspond to a systematic upwards increasing temperature gradient (i.e. inverted temperature gradient) within the MCTZ. This observation is in good agreement with other records of inverted field gradients in the MCTZ from different parts of the Himalayas (e.g. Hubbard, 1989; Pêcher, 1989; Metcalfe, 1993; Vannay and Grasemann, 1998). Furthermore, investigations using deformation mechanism and metamorphic reactions from orthogneiss mylonites of the same tectonic position from the Kumaun Himalayas support the interpretation of an inverted thermal profile (Srivastava and Mitra, 1996).

(3) The asymmetry of textures confirms the overall observed top-to-the-SW sense of shear.

(4) $\langle a \rangle$-axis from the upper structural levels of the MCTZ reveal pronounced single maxima oblique to *X*, suggesting one single predominant flow plane. By contrast, textures from the lower structural levels display two maxima, which are roughly symmetrically oriented around *X*. These results are interpreted by an increasing influence of coaxial flow towards lower structural levels.

(5) Modeling of Lister and Hobbs (1980) suggest that central girdle of quartz *c*-axes patterns develops orthogonal to the flow plane in both simple shear and pure shear. It has been suggested that the central girdle will also form perpendicular to the flow plane during general shear deformation (Platt and Behrmann, 1986; Vissers, 1989; Law et al., 1990; Wallis, 1992). Under these assumptions the angle between the perpendicular to the central girdle and the foliation (β) is equal to the angle between the flow plane and the flattening plane of strain (Fig. 10a). For steady-state plane strain isochoric deformation, this angle is a function of the vorticity and the finite strain. From the sine rule the rotation of the axes of the finite strain ellipsoid (θ), β and the ellipticity of the finite strain ellipsoid (R_f) can be related (Wallis, 1992):

$$\tan\theta = \frac{\sin 2\beta}{\dfrac{R_f+1}{R_f-1} - \cos 2\beta}. \tag{6}$$

Using the trigonometric relationship in the Mohr space, W_m can be related to R_f and θ:

$$W_m = \sin\theta \frac{R_f+1}{R_f-1}. \tag{7}$$

Therefore W_m can be calculated if R_f and β are known by eliminating θ from Eqs. (6) and (7) and simplifying:

$$W_m = \frac{C\sin 2\beta}{\left((C-\cos 2\beta)\sqrt{1+\dfrac{\sin^2 2\beta}{(C-\cos^2 2\beta)}}\right)}, \tag{8}$$

where:

$$C = \frac{R_f+1}{R_f-1}.$$

Similar, Eqs. (6) and (7) can be easily solved for β and the result can be plotted for different W_m (Fig. 10b):

$$\beta = \sin^{-1}\left\{\frac{(C^2 - W_m^2)\left(\sqrt{-\frac{C^2 W_m^2 (W_m^2 - 1)}{(C^2 - W_m^2)^2}}\sqrt{1 - \frac{W_m^2}{C^2}} - W_m\right)}{C^2\sqrt{1 - \frac{W_m^2}{C^2}}}\right\}. \quad (9)$$

This plot can be used to evaluate the reliability of quantitative kinematic studies applied to quartz texture analysis using the above mentioned assumptions. If the finite strain is low ($\sim R_f < 5$) and well constrained and if β can be determined within an error of $\pm 2^\circ$, quantitative estimates of W_m can be made within a limit of approximately 0.2–0.4 (e.g. Wallis, 1992). However, the limitation of most practical finite strain measurements and quartz texture analyses will only allow distinction between pure shear, pure shear dominated, simple shear dominated or nearly ideal simple shear flow. Analysis of simple shear dominated flows will be more accurate because the curves for higher W_m are more widely spaced than for low W_m. For large finite strains the method becomes less efficient because the curves for different W_m get closer spaced and asymptotically approach the abscissa. For $R_f > 20$, β is less than 5° for W_m ranging from 0 to 0.9. Only ideal simple shear will result in an angle between the line perpendicular to the central girdle and the foliation which is larger than 10°. Therefore, for large strain only three conditions may be realistically distinguished: (i) Pure shear with central girdles normal to the foliation (e.g. Type I crossed girdles). (ii) General shear with small β angles. However, within the errors of the methods it will be impossible to estimate W_m. (iii) Ideal simple shear with β angles larger than 10°. Therefore, this quantitative approach does not contribute much more information than the qualitative evaluation of the *c*- and ⟨*a*⟩-axis fabric topologies (Lister and Williams, 1979; Schmid and Casey, 1986).

For the presented *c*-axes patterns we suggest the following interpretations (Fig. 10): The asymmetry characterized by the angle β can be determined with sufficient accuracy using X-ray texture goniometry. However, we have no constraints on the absolute values of R_f. Given the large displacement along the MCTZ, the R_f values should be large. The highest β angles of around 13° have been found in the uppermost structural levels. This could be interpreted as a general shear flow ($0.4 < W_m < 0.9$) at small finite strains ($R_f < 6$). More realistically, because of the large displacement accommodated by the MCTZ, the flow has been close to simple shear at high finite strains ($R_f > 20$). The asymmetry decreases toward lower structural levels, resulting in β angles around 5° at the basal parts of the MCTZ. Regardless of the values of R_f, this implies a downward increasing pure shear component (note that in addition, decrease in W_m is qualitatively suggested by the shift from oblique girdles towards Type I cross girdle distributions). However, we have no control whether the finite strain at lower structural levels is in the same order as the R_f values at the top of the MCTZ. A finite strain profile (FSP) across the MCTZ, which records roughly similar values for R_f, would indicate W_m values around 0.9 at the base and 1.0 at the top of the shear zone (FSP-A in Fig. 10b). If the R_f value decreases towards the base of the MCTZ (FSP-B in Fig. 10b), then lower values for W_m are possible. Considering that higher-grade metamorphic rocks are exposed towards higher structural levels and consequently experienced a higher total exhumation (Grasemann and Vannay, 1999), we favor FSP-B, which is independently supported by petrological and structural arguments (Vannay and Grasemann, 1998).

4. Discussion

4.1. Implications for a decelerating deformation path

Fossen and Tikoff (1997) demonstrated that for steady-state deformation, simple shear produces a smaller finite strain than pure shear for an identical offset. The finite strain is minimized by a simultaneous combination of simple shear and pure shear (i.e. *minimum strain path*) or, in other words a general shear is the most effective strain history at accumulating offset for a given strain. Comparing a minimum strain path for the same boundary conditions of a non-steady-state and a steady-state flow, the mean vorticity number will be the same for both types of deformation paths. However, the non-steady-state deformation will start to deform close to ideal simple shear, and with increasing offset pure shear dominated deformation will compensate for the early simple shear flow. Although the finite strain ellipse is identical for the two cases, the deformation history is not (Fossen and Tikoff, 1997). Note that Jiang (1998) demonstrated that different quantities could be regarded as some measure of a shear zone displacement. However, the boundary condition of a thrust zone with a deformed hanging wall, but where the strain is decoupled from

the footwall by discontinuous deformation along a detachment, best approximates thrusting along the MCTZ and therefore we follow the definition of Fossen and Tikoff (1997).

Independently, Simpson and De Paor (1997) suggested that in most compressional orogenic belts it is likely that shear zones below the brittle layer deform by general shear flow. Using finite strain measurements and vorticity analysis of mylonites of a thrust in the Swedish Caledonides they showed that the quantitative kinematic indicators record a considerable greater pure shearing component than is recorded by the finite strain markers. They concluded that the deformation in the thrust most likely commenced as a predominantly simple shearing that became progressively more pure shear influenced at higher strains, culminating in predominantly pure shearing towards the final stage of deformation. They called this special type of deformation path, where the kinematic vorticity number is reduced as deformation proceeds, a *decelerating strain path*.

In the following it will be argued that, based on the quantitative flow studies presented above, the MCTZ deformed with an increasing pure shear component following a decelerating strain path. However, we avoid the description of the deformation history of the MCTZ as a minimum strain path because we have no control whether the recorded flow actually resulted in a minimum finite strain.

Accepting the above discussed assumptions, quantitative analysis of tension gashes and associated fringe folds of the MCTZ indicate a pure shear component during this stage of flow of more than 50%. The veins are abundant and occur throughout the MCTZ, crosscutting the earlier formed mylonitic fabric and the quartz layers from which the samples for texture investigations were taken. Clearly these structures overprint the mylonitic foliation and thus the derived mean vorticity number characterizes only this late stage of the ductile flow. A strong pure shear component is also confirmed by quartz *c*- and ⟨*a*⟩-axes pole diagrams from the structurally lower parts of the MCTZ, as indicated by crossed girdles with small internal or external asymmetries. However, at higher structural position, the quartz textures developed an obliquity of the central girdle segment with respect to the foliation trace as well as an unequal inclination of the peripheral legs with respect to the central girdle segment suggesting increasing importance of a non-coaxial deformation close to simple shear. Furthermore, the interpretation of the dominant slip systems reveals an increasing temperature from the bottom to the top of the MCTZ. Thus the quartz textural patterns indicate dominant simple shear deformation formed at higher temperatures than those indicating pure shear. Note that the quartz textures record an earlier stage of flow

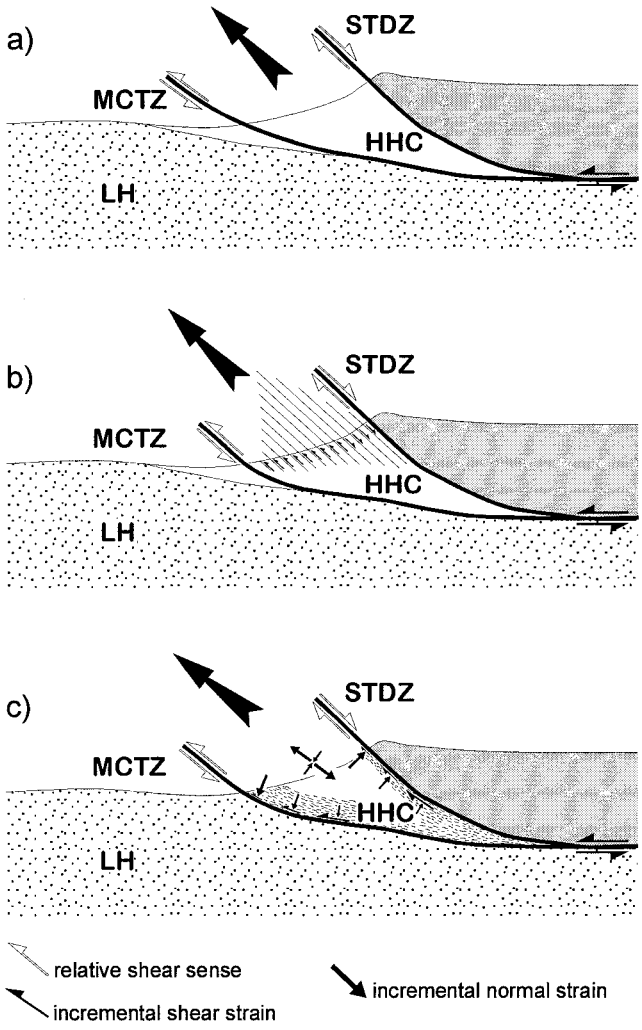

Fig. 11. Schematic models for a tectonically extruding wedge (HHC) bounded by the MCTZ and the STDZ. (a) Extrusion is accommodated by shearing along distinct faults at the MCTZ and the STDZ (e.g. Hodges et al., 1993). (b) The wedge is pervasively ductily deformed by simple shearing (Grujic et al., 1996). (c) This work suggests that deformation is more concentrated on the boundaries of the wedge, which deform by general shear flow and probably follow a decelerating strain path. Due to strain compatibility the center of the wedge extrudes mainly by pure shearing.

since the quartz layers are crosscut by the veins which have been used as quantitative kinematic indicators for the late stage of the deformation. These observations can be interpreted as a deformation history dominated at higher metamorphic conditions by simple shear flow, which is replaced by pure shear dominated flow at lower temperature conditions indicating a decelerating strain path.

Note that the distribution of the observed quartz textures from the MCTZ could also be interpreted by spatial variation of the flow type. Deformation at the different structural levels within the MCTZ may have formed at the same time but simple shear was localized to where the temperature was higher and consequently

the rocks were less competent. However, in this case the palaeogeothermal gradient must have been inverted, for which no evidence has been found within this section of the MCTZ (Vannay and Grasemann, 1998). Therefore, we favor the idea that the observed distribution of the deformation pattern was caused by temporal variations in flow type.

4.2. Extrusion of crustal wedges

The decelerating strain path with an increasing pure shear flow at the late stage of the MCTZ thrusting bears important consequences for Early Miocene tectonic history of the Himalayas, especially the extrusion of the HHC wedge.

Using the concept of strain compatibility, parallel-sided shear zones can only deform by (i) simple shear with shear plane orientations parallel to the walls, (ii) heterogeneous volume change with volumetric change developed by displacements perpendicular to the shear zone walls, (iii) uniform homogeneous general shear affecting the shear zone and its walls, or (iv) any combination of these processes (Ramsay and Graham, 1970). Shear zones with unstrained walls, but where the walls are not parallel sided, will result in extrusive motion of the material in the shear zone deforming with heterogeneous general shear (Ramsay and Huber, 1987). In other words, general shear always occurs if the wall rock itself undergoes deformation and/or if the shear zone boundaries are not parallel sided.

It has been suggested that large-scale thrusting at the base of the MCTZ occurred simultaneously with normal faulting along the STDZ at the top of the HHC along much of the Himalayan orogen (e.g. Burchfiel et al., 1992; Hodges et al., 1992). Therefore the HHC can be modeled as a southwards extruding wedge between a thrust at the base and a normal fault at the top (e.g. Burchfiel and Royden, 1985; Hodges et al., 1993; Grujic et al., 1996). Note that geophysical data indeed indicate that the bounding faults are not parallel but converge downward (Nelson et al., 1996). Whereas earlier models assume that the main deformation is restricted to distinct faults at the bottom and the top of the wedge (Fig. 11a), field data suggest that the extruding wedge did not act as a rigid block, but was deformed during extrusion (Fig. 11b) with strain concentration at the bottom and the top (Grujic et al., 1996).

The quantitative kinematic indicators presented in this study derived from the basal mylonites of the HHC indicate a non-steady-state general shear flow following a decelerating strain path. The pure shear component of deformation requires that some elongation of the general shear zone must exist. This elongation can be either accommodated by pure shear deformation of the wall rock or by discontinuous deformation along a detachment or stretching fault (Means, 1989; Fossen and Tikoff, 1997). In case of the investigated orthogneiss mylonites, strain compatibility requirements must be relaxed at the base because the whole MCTZ is detached from the underlying LH along brittle faults. However, there is no detachment between the highly strained orthogneiss mylonites and the overlying less-strained schists and paragneisses of the HFm. In order to maintain strain compatibility, the Haimanta Formation should record a strong elongation component about the magnitude of the pure shear component of the MCTZ. Even though this ideal geometric model cannot be easily quantified in the field, the HFm frequently shows symmetric boudinage and conjugate shear-band overprinting the older fabric, suggesting a late-stage strong SW–NE stretching component. Although this study is focused on the mylonites of the MCTZ at the base of the extruding wedge of the HHC and higher structural levels are not exposed in the investigated section, a hypothetical modification of the flow within the deforming crustal wedge is suggested (Fig. 11c).

The late ductile to brittle–ductile deformation of the MCTZ reveals a strong pure shear component. Earlier flow at higher temperatures was probably closer to simple shear, suggesting a decelerating strain path. At the lower boundary of the MCTZ, a detachment (stretching fault) allows discontinuous deformation. However, for the material above the MCTZ, strain compatibility must be maintained and consequently the center of the wedge accommodates the pure shear component of the flow of the MCTZ by elongation. If the STDZ on top of the wedge deforms as well by general shear flow, the stretching component parallel to the normal fault is detached from the hanging wall, but due to strain compatibility again induces an elongation within the middle part of the wedge. Thus general shear flow within the thrust at the bottom and the normal fault at the top of a crustal wedge enhances the extrusion component of the central part of the wedge. This result is in good agreement with field observations where the central part of the wedge records the highest metamorphic conditions (e.g. Hodges et al., 1993; Grujic et al., 1996). Note that, depending on the total displacement, the thickness of the shear zones and the flow type within the bounding thrust and the normal fault, the highest metamorphic conditions do not necessarily have to occur in the center of the wedge (Vannay and Grasemann, 1998).

In this study only the flow from the MCTZ has been studied. However, the finite displacement path within an extruding wedge has important consequences on the interpretation of metamorphic pressure–temperature–time paths and cooling histories of rocks. Therefore a more rigorous study of the flow parameters across the whole extruding wedge would con-

tribute to a better understanding of the kinematics of the exhumation of the HHC in future studies.

5. Conclusions

1. Fringe folds develop near tension gashes due to rotation of veins and preservation of an existing foliation in the vicinity of the veins. These structures are useful quantitative kinematic indicators, which record a late ductile stage of flow.
2. The interpretation of the angle between the normal to the central girdle and the foliation from quartz *c*-axis pole figures in terms of flow parameters have to be used cautiously. For large strains this angle would be less than 5° for flows with mean vorticity numbers between 0 and 0.9. For ideal simple shear β is above 10° even at high strain.
3. Quartz *c*-axis pole figure plots from the MCTZ reveal a systematic change of the preferred slip systems from prism $\langle a \rangle$ glide (upper structural levels of the MCTZ) to rhomb $\langle a \rangle$ glide towards contributions of basal $\langle a \rangle$ glide in MCTZ footwall units. Our interpretation of higher syn-deformative temperatures within upper structural levels and lower temperatures within lower structural levels of the MCTZ is in agreement with similar results derived by different methods from other parts of the MCTZ.
4. The interpretation of quartz textures from mylonitic orthogneisses from the MCTZ, which are overprinted by the fringe folds suggest that deformation at higher temperatures had a stronger degree of non-coaxiality than deformation at lower temperatures. This observation suggests that the flow within the MCTZ probably followed a decelerating strain path.
5. A hypothetical model representing a modification of existing models, which explain the exhumation of the HHC as a southwards extruding wedge between the MCTZ and the STDZ, is suggested. Both shear zones at the top and the base of the wedge have a pronounced pure shear component, especially at the late stage of ductile flow, and probably followed a decelerating strain path. Whereas deformation within these shear zones is decoupled from the hanging wall and the footwall by detachments, the central part of the wedge has to deform with a strong pure shear component in order to maintain the requirements of strain compatibility.

Acknowledgements

We thank Christine Miller and Gerhard Wiesmayr for assisting the fieldwork and sample collection, and Hugh Rice, Djorde Grujic, Neil Mancktelow, Erich Draganits and Wofgang Frank for fruitful discussions. We acknowledge support from the Austrian 'Fond zur Förderung der wissenschaftlichen Forschung' (FWF grant P-11765-GEO). We thank an anonymous reviewer for comments and Haakon Fossen for a very careful review and important suggestions. A special 'thank you' to Cees Passchier for sending us a copy of his manuscript about 'fringe structures' which is currently under review.

References

Bobyarchick, A.R., 1986. The eigenvalues of steady flow in Mohr space. Tectonophysics 122, 35–51.

Bouchez, J.L., 1977. Plastic deformation of quartzites at low temperatures in an area of natural strain gradient. Tectonophysics 39, 25–50.

Bunge, H.J., 1969. Mathematische Methoden der Texturanalyse. Akademie, Berlin.

Burchfiel, B.C., Royden, L.H., 1985. North south extension within the convergent Himalayan region. Geology 13, 679–682.

Burchfiel, B.C., Zhiliang, C., Hodges, K.V., Yuping, L., Royden, L.H., Changrong, D., Jiene, X., 1992. The southern Tibetan detachment system, Himalayan Orogen: extension contemporaneous with and parallel to shortening in a collisional mountain belt. Geological Society of America Special Paper 269, 1–41.

Burg, J.P., Brunel, M., Gapais, D., Chen, G.M., Liu, G.H., 1984. Deformation of leucogranites of the crystalline Main Central Sheet in southern Tibet (China). Journal of Structural Geology 6, 535–542.

De Paor, D.G., Means, W.D., 1984. Mohr circles of the First and Second Kind and their use to represent tensor operations. Journal of Structural Geology 6, 693–701.

Dèzes, P.J., Vannay, J.-C., Steck, A., Bussy, F., Cosca, M., 1999. Synorogenic extension; quantitative constraints on the age and displacement of the Zanskar Shear Zone (NW-Himalaya). Geological Society of America Bulletin 111, 364–374.

Druguet, E., Passchier, C.W., Carreras, J., Victor, P., den Brock, S., 1997. Analysis of a complex high-strain zone at Cap de Creus, Spain. Tectonophysics 280, 31–45.

Fossen, H., Tikoff, B., 1997. Forward modeling of non-steady-state deformations and the 'minimum strain path'. Journal of Structural Geology 19, 987–996.

Fossen, H., Tikoff, B., 1998. Forward modeling of non-steady-state deformations and the 'minimum strain path': Reply. Journal of Structural Geology 20, 979–981.

Frank, W., Fuchs, G., 1970. Geological investigations in West Nepal and their significance for the geology of the Himalayas. Geologische Rundschau 59, 552–580.

Frank, W., Grasemann, B., Guntli, P., Miller, Ch., 1995. Geological map of the Kishtwar–Chamba–Kulu region (NW Himalayas, India). Jahrbuch der Geologischen Bundesanstalt 138, 299–308.

Gosh, S.K., Ramberg, H., 1976. Reorientation of inclusions by combination of pure and simple-shear. Tectonophysics 34, 1–70.

Grasemann, B., Vannay, J.-C., 1999. Flow controlled inverted metamorphism in shear zones. Journal of Structural Geology 21, 743–750.

Grujic, D., Casey, M., Davidson, C., Hollister, L.S., Kündig, R., Pavlis, T., Schmid, S., 1996. Ductile extrusion of the Higher Himalayan Crystalline in Bhutan: evidence from the quartz microfabrics. Tectonophysics 260, 21–43.

Herwegh, M., Handy, M.R., 1998. The origin of shape preferred

orientations in mylonite: inferences from in-situ experiments on polycrystalline norcamphor. Journal of Structural Geology 20, 681–694.

Hodges, K.V., Parrish, R.R., Housh, T.B., Lux, D.R., Burchfiel, B.C., Royden, L.H., Chen, Z., 1992. Simultaneous Miocene extension and shortening in the Himalayan orogen. Science 258, 1466–1470.

Hodges, K.V., Burchfiel, B.C., Royden, L.H., Chen, Z., Liu, Y., 1993. The metamorphic signature of contemporaneous extension and shortening in the central Himalayan orogen: data from Nyalam transect, southern Tibet. Journal of Metamorphic Geology 11, 721–737.

Hodges, K., Bowring, S., Davidek, K., Hawkins, D., Krol, M., 1998. Evidence for rapid displacement on Himalayan normal faults and the importance of tectonic denudation in the evolution of mountain ranges. Geology 26, 481–576.

Hubbard, M.S., 1989. Thermobarometric constraints on the thermal history of the Main Central Thrust Zone and Tibetan Slab, eastern Nepal Himalaya. Journal of Metamorphic Geology 7, 19–30.

Hudleston, P.J., 1989. The association of folds and veins in shear zones. Journal of Structural Geology 11, 949–957.

Jiang, D., 1998. Forward modeling of non-steady-state deformations and the 'minimum strain path': Discussion. Journal of Structural Geology 20, 975–977.

Jiang, D., White, J.C., 1995. Kinematics of rock flow and the interpretation of geological structures with particular reference to shear zones. Journal of Structural Geology 17, 1249–1266.

Law, R.D., 1990. Crystallographic fabrics: a selective review of their applications to research in structural geology. In: Knipe, R.J., Rutter, E.H. (Eds.), Deformation Mechanisms, Rheology and Tectonics, Special Publication 54. Geological Society of London, pp. 335–352.

Law, R.D., Schmid, S.M., Wheeler, J., 1990. Simple-shear deformation and quartz crystallographic fabrics: a possible natural example from the Torridon area of NW Scotland. Journal of Structural Geology 12, 29–45.

Lister, G.S., Dornsiepen, U.F., 1982. Fabric transition in the Saxony granulite terrain. Journal of Structural Geology 1, 283–298.

Lister, G.S., Hobbs, B.E., 1980. The simulation of fabric development during plastic deformation and its application to quartzite: the influence of deformation history. Journal of Structural Geology 2, 355–370.

Lister, G.S., Williams, P.F., 1979. Fabric development in shear zones: theoretical controls and observed phenomena. Journal of Structural Geology 1, 283–297.

Means, W.D., 1982. An unfamiliar Mohr Circle construction for finite strain. Tectonophysics 89, T1–T6.

Means, W.D., 1989. Stretching faults. Geology 17, 893–896.

Merle, O., 1986. Patterns of stretch trajectories and strain rates within spreading-gliding nappes. Tectonophysics 124, 211–222.

Metcalfe, R.P., 1993. Pressure, temperature and time constraints on metamorphism across the Main Central Thrust zone and High Himalayan Slab in the Garhwal Himalaya. In: Treloar, P.J., Searle, M.P. (Eds.), Himalayan Tectonics, Special Publication 74. Geological Society, pp. 485–510.

Nelson, K.D., et al., 1996. Partially molten middle crust beneath southern Tibet: synthesis of project INDEPTH results. Science 274, 1684–1688.

Olson, J.E., Pollard, D.D., 1991. The initiation and growth of en échelon veins. Journal of Structural Geology 13, 595–608.

Passchier, C.W., 1986. Flow in natural shear zones—the consequences of spinning flow regimes. Earth and Planetary Science Letters 77, 70–80.

Passchier, C.W., 1987. Stable positions of rigid objects in non-coaxial flow—a study in vorticity analysis. Journal of Structural Geology 9, 679–690.

Passchier, C.W., 1988. The use of Mohr circles to describe non-coaxial progressive deformation. Tectonophysics 149, 323–338.

Passchier, C.W., 1990. Reconstruction of deformation and flow parameters from deformed vein sets. Tectonophysics 180, 185–199.

Passchier, C.W., 1997. Vein-margin folds. EUG Abstract Supplement Terra Nova 9, 373.

Passchier, C.W., Trouw, R.A.J., 1996. Microtectonics. Springer-Verlag, Berlin.

Passchier, C.W., Urai, L., 1988. Vorticity and strain analysis using the Mohr diagrams. Journal of Structural Geology 10, 755–763.

Pêcher, A., 1989. The metamorphism in the central Himalaya. Journal of Metamorphic Geology 7, 31–41.

Platt, J.P., Behrmann, J.H., 1986. Structures and fabrics in a crustal-scale shear zone, Betic Cordillera, SE Spain. Journal of Structural Geology 8, 15–33.

Platt, J.P., Vissers, R.L.M., 1980. Extensional structures in anisotropic rocks. Journal of Structural Geology 2, 397–410.

Poirier, J.P., 1980. Shear localization and shear instability in materials in the ductile field. Journal of Structural Geology 2, 135–142.

Ramsay, J.G., Graham, R.H., 1970. Strain variation in shear belts. Canadian Journal of Earth Science 7, 786–813.

Ramsay, J.G., Huber, M.I., 1983. The Techniques of Modern Structural Geology, Volume 1: Strain Analysis. Academic Press, London.

Ramsay, J.G., Huber, M.I., 1987. The Techniques of Modern Structural Geology, Volume 2: Folds and Fractures. Academic Press, London.

Rice, A.H.N., 1986. Structures associated with superimposed inhomogeneous shearing of basic dykes from Finnmark, Norway. Tectonophysics 128, 61–75.

Roe, R.J., 1965. Description of crystallite orientation of polycrystalline materials. II. General solution to pole figure inversion. Journal of Applied Physics 37, 2069–2072.

Schmid, S.M., Casey, M., 1986. Complete fabric analysis of some commonly observed quartz *c*-axis patterns. Geophysical Monograph, American Geophysical Union 36, 263–286.

Simpson, C., De Paor, D., 1993. Strain and kinematic analysis in general shear zones. Journal of Structural Geology 15, 1–20.

Simpson, C., De Paor, D.G., 1997. Practical analysis of general shear zones using the porphyroclast hyperbolic distribution method: An example from the Scandinavian Caledonides. In: Sengupta, S. (Ed.), Evolution of Geological Structures in Micro- to Macro-scales. Chapman & Hall, London, pp. 169–184.

Srivastava, P., Mitra, G., 1996. Deformation mechanism and inverted thermal profile in the North Almora Thrust mylonite zone, Kumaon Lesser Himalaya, India. Journal of Structural Geology 18, 27–39.

Thöni, M., 1977. Geology, structural evolution and metamorphic zoning in the Kulu Valley (Himachal Himalayas, India) with special reference to the reversed metamorphism. Mitteilung der Gesellschaft der Geologie und Bergbaustudenten in Österreichs 24, 125–187.

Tikoff, B., Fossen, H., 1993. Simultaneous pure and simple-shear: the unifying deformation matrix. Tectonophysics 217, 267–283.

Trivedi, J.R., Gopalan, K., Valdiya, K.S., 1984. Rb–Sr ages of granitic rocks within the Lesser Himalayan nappes, Kumaun, India. Journal of the Geological Society of India 26, 641–654.

Truesdell, C., 1954. The Kinematics of Vorticity. Indiana University Press, Bloomington, Indiana.

Vannay, J.-C., Grasemann, B., 1998. Himalayan inverted metamorphism in the High Himalaya of Kinnaur (NW India) petrography versus thermobarometry. Schweizer mineralogische und petrographische Mitteilungen 78, 107–132.

Vissers, R.L.M., 1989. Asymmetric quartz *c*-axis fabric and flow vor-

ticity: a study using rotated garnets. Journal of Structural Geology 11, 231–244.
Wallis, S.R., 1992. Vorticity analysis in a metachert from the Sanbagwa Belt, SW Japan. Journal of Structural Geology 14, 271–280.
Wenk, H.-R., 1985. Measurement of pole figures. In: Wenk, H.-R. (Ed.), Preferred Orientation in Deformed Metals and Rocks. Academic Press, Orlando, pp. 11–47.
West, W.D., 1939. The structure of the Shali "window" near Simla. Records of the Geological Survey of India 74, 133–167.
Wilson, C.J.L., 1975. Preferred orientation in quartz ribbon mylonites. Geological Society of America Bulletin 86, 968–974.